Electronic Supplementary Material (ESI) for Physical Chemistry Chemical Physics.

Supplemental Material:

Optical spectra and exciton lifetimes in bulk transition metal dichalcogenides

Cesar E. P. Villegas,[1,*] Enesio Marinho Jr,[2,†] Pedro Venezuela,[3,‡] and Alexandre R. Rocha[2,§]

[1] *Departamento de Ciencias, Universidad Privada del Norte, Lima 15434, Peru*

[2] *Instituto de Física Teórica, Universidade Estadual Paulista (UNESP), R. Dr. Bento Teobaldo Ferraz, 271, São Paulo, 01140-070 São Paulo, Brazil.*

[3] *Instituto de Física, Universidade Federal Fluminense (UFF), Av. Gal. Milton Tavares de Souza, s/n, 24210-346 Niterói, Rio de Janeiro, Brazil.*

[*] cesar.perez@upn.edu.pe

[†] enesio.marinho@unesp.br

[‡] pedrovenezuela@id.uff.br

[§] alexandre.reily@unesp.br

I. CONVERGENCE TESTS FOR GW CALCULATIONS

The Fig. S1 and S2 show the convergence of the *GW* parameters at Γ, and *K* point with respect to the number of bands in the self-energy, screened cutoff, number of bands in the dielectric matrix, and the *k*-grid sample. To achieve convergence, we follow the stategy proposed in Ref. [1]. It involves to keep other parameters at maximum values to prevent their influence on the analyzed parameter. On the basis that the converged parameters resulting from summations over bands and **G** vectors may not significantly be altered with the **k**− points [1], we reduce our sampling to a Γ−centered $3 \times 3 \times 1$ during the convergence procedure. To determine the converged energy cutoff for the dielectric matrix, the number of bands in both the self-energy and dielectric function is set to 3000. After establishing the converged number of **G**-vectors of 30 Ry for the dielectric matrix, we employ this value and reset the number of bands in the self-energy to infinity (3000), while adjusting the number of bands in the dielectric matrix.

The appropriated number of **G**−vectors in the exchange part of the self-energy was estimated by setting both the number bands in W and Σ^c to infinity, and a screening cutoff of 30 Ry. Finally, to address the convergence of the number of bands in the self-energy (Σ^c), we employ 3000 bands in W with a screening cutoff of 30 Ry and 60 Ry in Σ^x.

For converging the **k**−point mesh we employ the already converged parameters for the number of bands in self-energy, number of bands in the dielectric matrix, and the screening cutoff, while we estimate the error in the quasiparticle gap at K and Γ point as the **k**−point sampling is varied. Our GW calculations present reliable predictions within an accuracy of ∼50 meV at K point and for all the cases.

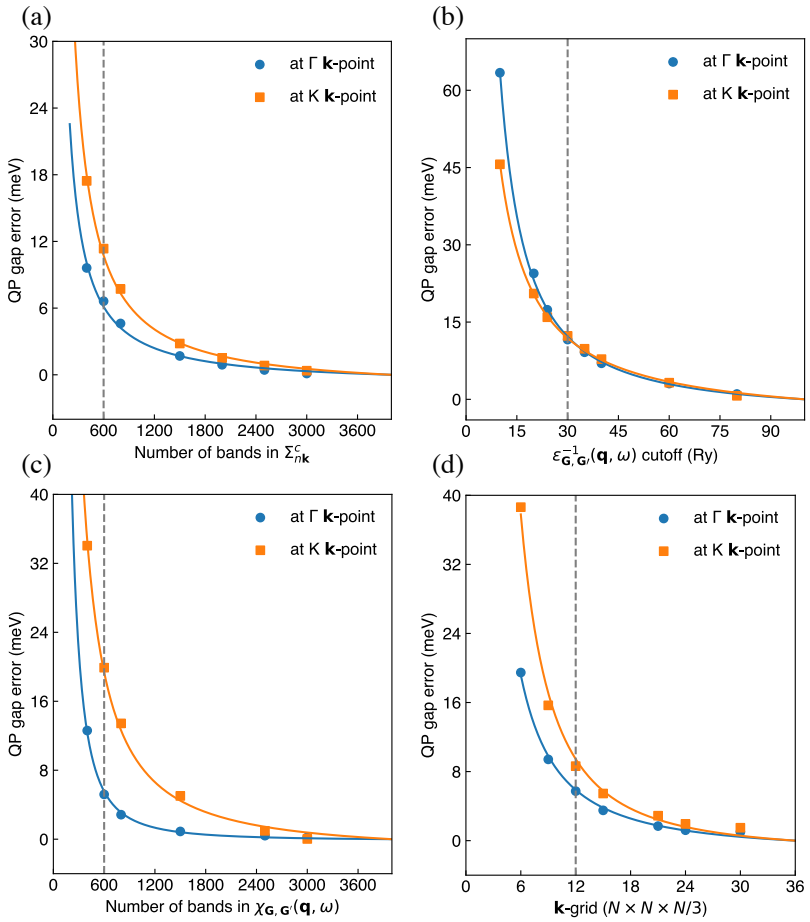

FIG. S1. Convergence of GW parameters for bulk 2H-MoS_2, with respect to (a) number of bands in the correlation part of self-energy operator, (b) number of **G**-vectors (energy cutoff) in the dielectric matrix, (c) number of bands to construct the response function, and (d) **k**-grid sampling. The error in quasiparticle (QP) direct band gap is computed at **k**-points Γ and K. The dashed lines represent the values chosen for each GW parameter.

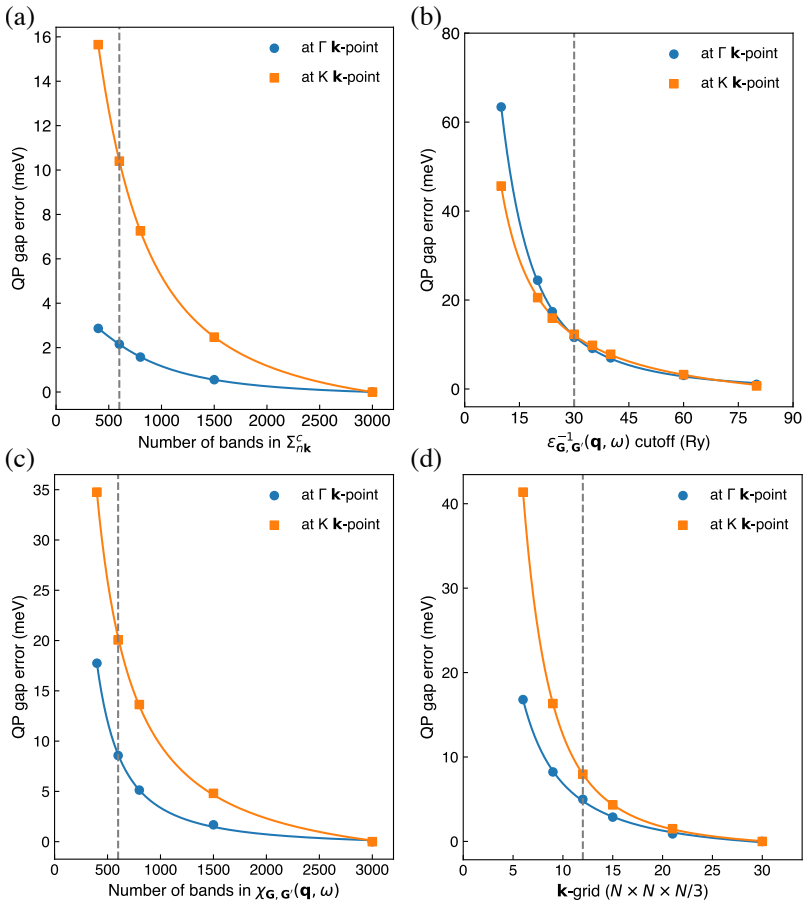

FIG. S2. Convergence of GW parameters for bulk 2H-WS_2, with respect to (a) number of bands in the correlation part of self-energy operator, (b) number of **G**-vectors (energy cutoff) in the dielectric matrix, (c) number of bands to construct the response function, and (d) **k**-point grid. The error in quasiparticle (QP) direct band gap is computed at **k**-points Γ and K. The dashed lines represent the chosen values for each GW feature.

II. CONVERGENCE TESTS FOR BETHE SALPETER CALCULATIONS

In Figs. S3 and S4 we present the convergence test for the BSE parameters. We mention that the BSE-Kernel is constructed based on the static screening. In this regard, in the upper pannels of both figures, we test the convergence of the BSE spectrum with respect to the energy cutoff and number of bands in the attractive direct screened Coulomb term. The bottom pannels, show the convergence of the BSE spectrum with respect to the exchange part of the BSE kernel (left) and the the k-grid sample (right). For simplicity, during the convergence tests, we ommited the spin-orbit coupling.

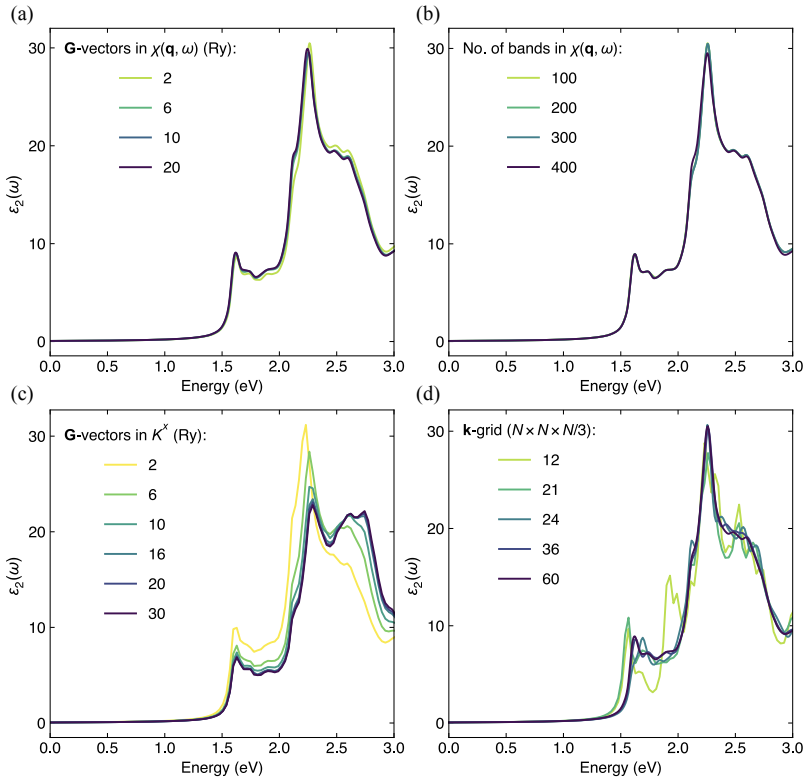

FIG. S3. Convergence of BSE optical absorption spectrum of bulk 2H-MoS_2 as a function of (a) number **G**-vectors and (b) number of bands in the screening, (c) **G**-vectors in the electron-hole exchange part K^x, and (d) **k**-point sampling.

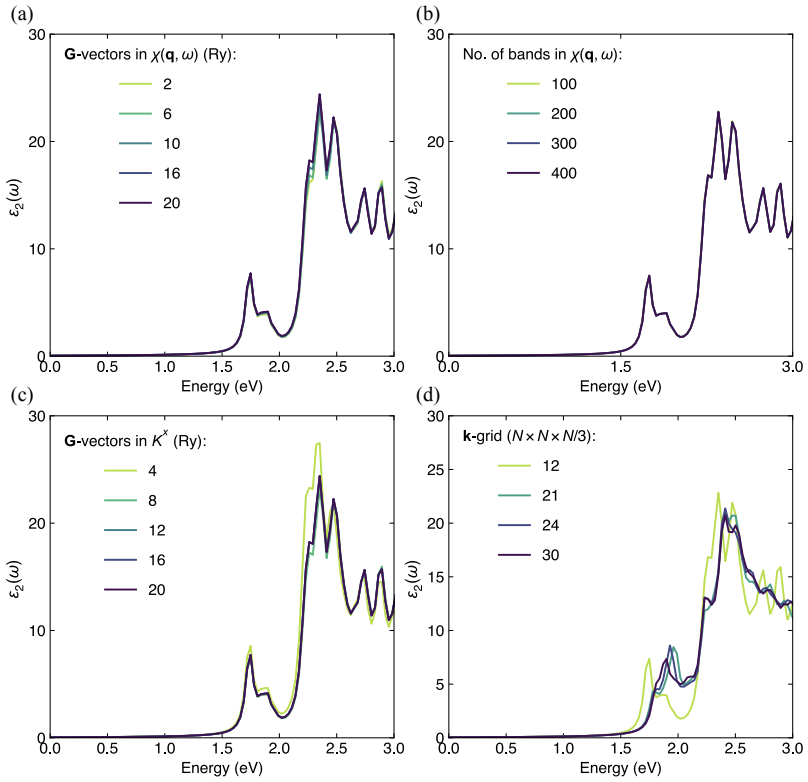

FIG. S4. Convergence of BSE optical absorption spectrum of the bulk 2H-WS_2 as a function of (a) number **G**-vectors and (b) number of bands in the screening, (c) **G**-vectors in the electron-hole exchange part K^x, and (d) **k**-point sampling.

III. DIRECT DARK EXCITON WAVEFUNCTIONS IN BULK TMDCS

Fig. S5 shows the exciton wave function distribution for the studied bulk TMDCs. Here the red arrows indicate the position of the hole. In all cases, the wavefunction spreads largely within the plane the hole belongs, which suggest its intralayer character. In all cases, the density in neighboring layers small.

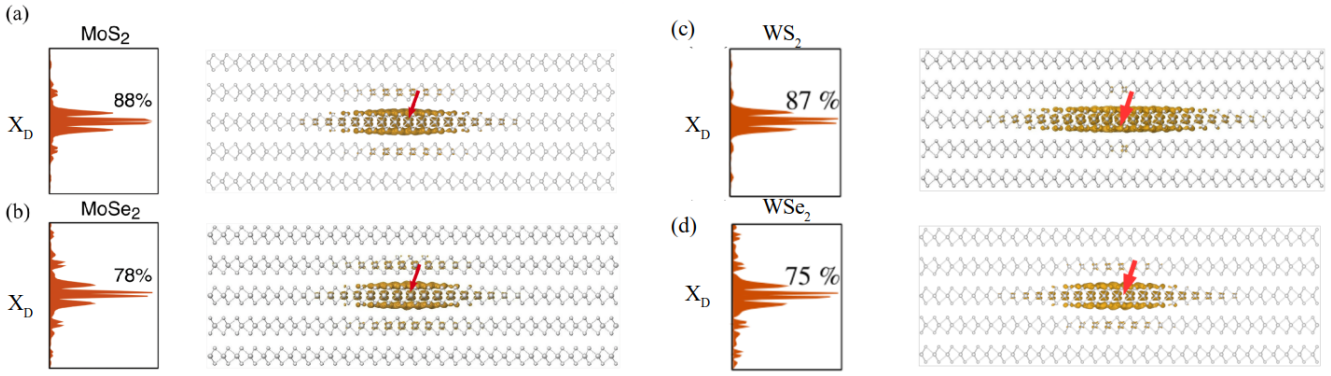

FIG. S5. Real space-projected exciton wave functions in bulk Mo- and W-based 2H-TMDCs: side view of dark exciton X_{D} in (a) MoS_2, (b) $MoSe_2$, (c) WS_2, and (d) WSe_2. In all the cases, the hole has been placed on the Mo(W) atom in the center of the figure as indicated by the red arrows. The left panels show the integrated projection along **c** axis, as well as the percentual contribution of the central layer as a fraction of the total electron probability distribution.

IV. BAND STRUCTURES AT THE GROUND STATE LEVEL

In Fig. S6 we present the ground state band structure of $MoSe_2$ with and without including spin-orbit coupling (SOC) effects, as a representative case for highligthing the role of SOC in bulk TMDCs. Along the Γ-M-K-Γ the effects of SOC is neglible in bulk systems. However, in the out-of-plane direction, in particular around H-point, the SOC effects splits the highest energy valence band.

In Figure S7 we present a comparison of the quasiparticle band structure with the ground state ones for $MoSe_2$ and WS_2.

In Figure S8 it is presented the spin-resolved band structure for MoS_2 and WSe_2. Since in bulk TMDCs the spin is degerated at valence band maximum and conduction band minimum, we resolved the spin for the layer index. From this figure one can clearly observe that at K, and K' points, and for a given layer, the spin is inverted.

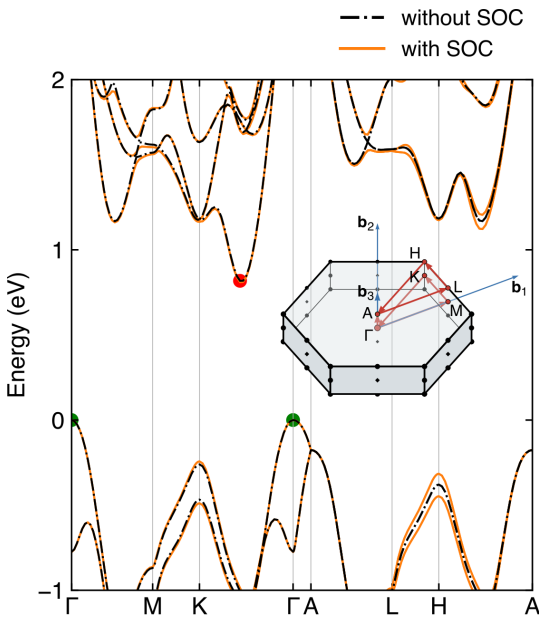

FIG. S6. Band structures of 2H-$MoSe_2$ without and with spin-orbit coupling at the PBE-D2 level. The green (red) circle indicates the position of the valence band maximum (conduction band minimum). The inset gives the locations of the symmetry **k**-points and symmetry lines in the first Brillouin zone.

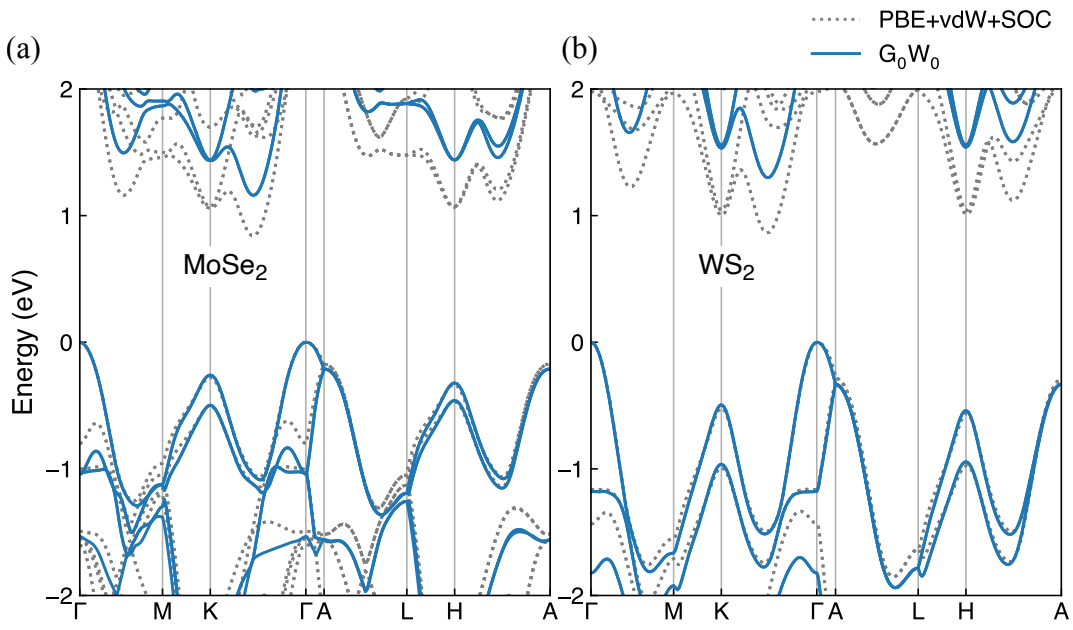

FIG. S7. Quasiparticle band structures for (a) 2H-$MoSe_2$ and (c) 2HWS_2. The DFT-PBE band structure, including van der Waals corrections and spin-orbit coupling is shown in grey dashed lines for comparison purposes.

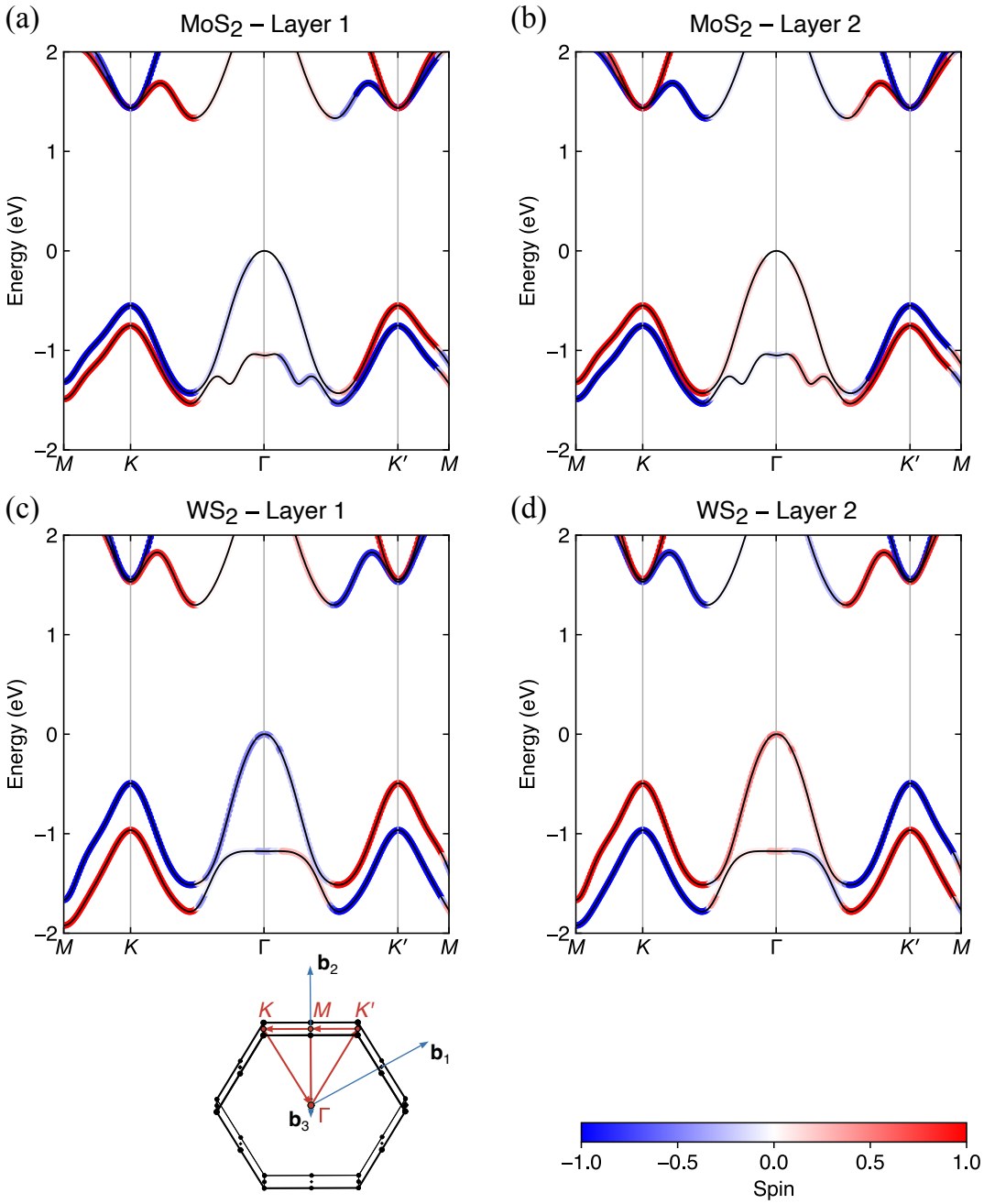

FIG. S8. Spin-resolved band structure for (a) 2H-MoS_2: layer 1 and (b) layer 2; and for (c) 2H-WS_2: layer 1 and (d) layer 2, both calculated within DFT-PBE level, including van der Waals corrections and spin-orbit coupling. The color scale indicates the expectation value of the spin projections for a given set of bands and **k**-point.

V. FEATURES FOR EXCITON RADIATIVE RATES, LATTICE CONSTANS

In table S1 we present the electronic structure parameters necessary for the simulation of the radiative lifetimes.

Table S2 presents the fully relaxed structural parameters of the studied systems.

TABLE S1. Features applied in the calculation of exciton radiative rates (Eq. 3 in main text) for the TMDCs: exciton eigenvalue $\Omega_{X_A}(0)$, volume V, in-plane (out-of-plane) exciton effective mass M_{xy} (M_z) in units of electron rest mass m_e, in-plane (out-of-plane) dielectric constant ϵ_{xy} (ϵ_z).

	MoS_2	$MoSe_2$	WS_2	WSe_2
$\Omega_{X_A}(0)$ (eV)	1.88	1.61	1.96	1.56
V (bohr^3)	739.5	839.0	722.6	834.6
M_{xy} (m_e)	1.04	1.36	0.68	0.74
M_z (m_e)	59.7	22.6	13.1	8.24
ϵ_{xy}[a]	15.9	17.7	14.4	15.9
ϵ_z[a]	6.90	8.5	6.4	7.8

TABLE S2. Fully-relaxed lattice parameters of bulk TMDCs obtained within DFT-PBE with van der Waals corrections and fully including spin-orbit interactions.

Lattice parameter (Å)	MoS_2	$MoSe_2$	WS_2	WSe_2
a	3.19	3.32	3.19	3.34
c	12.42	13.03	12.16	12.81

VI. INPUT FILES

Below we present the input files for self-consistent calculations of our bulk TMDCs.

&control
calculation =′scf′,
restart_mode=′from_scratch′,
prefix =′MoS2′,
tstress=.true.
tprnfor=.true.
pseudo_dir =′/Pseudos/′,
outdir=’./’,
nstep=500
forc_conv_thr=1.0D-6
/
&system
vdw_corr= ′Grimme-D2′,
ibrav = 4,
celldm(1)= 6.030418654,
celldm(3)= 3.894001681,
nat = 6,
ntyp = 2,
ecutwfc = 84,
lspinorb=.true.,
noncolin=.true.
/
&electrons
electron_maxstep = 100
conv_thr = 1.0d-11
mixing_mode = ’plain’
mixing_beta = 0.7
mixing_ndim = 8
diagonalization = ′david′
diago_david_ndim = 4
diago_full_acc = .true.
/

ATOMIC_SPECIES

Mo 95.94 Mo_ONCV_PBE_FR-1.1.upf

S 32.06 S_ONCV_PBE-1.1.upf

ATOMIC_POSITIONS (crystal)

S 0.333333000 0.666667000 0.124680075

S 0.666667000 0.333333000 0.624680073

S 0.333333000 0.666667000 0.375319927

S 0.666667000 0.333333000 0.875319925

Mo 0.666667000 0.333333000 0.250000047

Mo 0.333333000 0.666667000 0.749999953

K_POINTS (automatic)

8 8 4 0 0 0

&control

calculation =′*scf*′,

restart_mode=′from_scratch′,

prefix =′WSe2′,

tstress=.true.

tprnfor=.true.

pseudo_dir =′/*Pseudos*/′,

outdir='./',

nstep=500

forc_conv_thr=1.0D-6

/

&system

vdw_corr= ′Grimme-D2′,

ibrav = 4,

celldm(1)= 6.31,

celldm(3)= 3.836,

nat = 6,

ntyp = 2,

ecutwfc = 84,

lspinorb=.true.,

noncolin=.true.

/

&electrons

electron_maxstep = 100

conv_thr = 1.0d-11

mixing_mode = 'plain'

mixing_beta = 0.7

mixing_ndim = 8

diagonalization = 'david'

diago_david_ndim = 4

diago_full_acc = .true.

/

ATOMIC_SPECIES

W 183.84 W_ONCV_PBE_FR-1.1.upf

Se 78.97 Se_ONCV_PBE-1.1.upf

ATOMIC_POSITIONS (crystal)

Se 0.333333000 0.666667000 0.1198199710

Se 0.666667000 0.333333000 0.6198199710

Se 0.333333000 0.666667000 0.3801800290

Se 0.666667000 0.333333000 0.8801800290

W 0.666667000 0.333333000 0.2500000000

W 0.333333000 0.666667000 0.7500000000

K_POINTS (automatic)

8 8 4 0 0

```
    &control
calculation ='scf',
restart_mode='from_scratch',
prefix ='MoSe2',
tstress=.true.
tprnfor=.true.
pseudo_dir ='/Pseudos/',
outdir='./',
nstep=500
forc_conv_thr=1.0D-6
/
&system
vdw_corr= 'Grimme-D2',
ibrav = 4,
celldm(1)= ,
celldm(3)= ,
nat = 6,
ntyp = 2,
ecutwfc = 84,
lspinorb=.true.,
noncolin=.true.
/
&electrons
electron_maxstep = 100
conv_thr = 1.0d-11
mixing_mode = 'plain'
mixing_beta = 0.7
mixing_ndim = 8
diagonalization = 'david'
diago_david_ndim = 4
diago_full_acc = .true.
/
```

ATOMIC_SPECIES

Mo 95.94 Mo_ONCV_PBE_FR-1.1.upf

Se 78.97 Se_ONCV_PBE-1.1.upf

ATOMIC_POSITIONS (crystal)

S 0.333333000 0.666667000

S 0.666667000 0.333333000

S 0.333333000 0.666667000

S 0.666667000 0.333333000

Mo 0.666667000 0.333333000

Mo 0.333333000 0.666667000

K_POINTS (automatic)

8 8 4 0 0 0

&control

calculation =′*scf*′,

restart_mode=′from_scratch′,

prefix =′WS2′,

tstress=.true.

tprnfor=.true.

pseudo_dir =′/*Pseudos*/′,

outdir='./',

nstep=500

forc_conv_thr=1.0D-6

/

&system

vdw_corr= ′Grimme-D2′,

ibrav = 4,

celldm(1)= ,

celldm(3)= ,

nat = 6,

ntyp = 2,

ecutwfc = 84,

lspinorb=.true.,

noncolin=.true.

/

&electrons

electron_maxstep = 100

conv_thr = 1.0d-11

mixing_mode = 'plain'

mixing_beta = 0.7

mixing_ndim = 8

diagonalization = 'david'

diago_david_ndim = 4

diago_full_acc = .true.

/

ATOMIC_SPECIES

W 183.84 W_ONCV_PBE_FR-1.1.upf

S 32.06 S_ONCV_PBE-1.1.upf

ATOMIC_POSITIONS (crystal)

Se 0.333333000 0.666667000

Se 0.666667000 0.333333000

Se 0.333333000 0.666667000

Se 0.666667000 0.333333000

W 0.666667000 0.333333000

W 0.333333000 0.666667000

K_POINTS (automatic)

8 8 4 0 0

---

[1] B. D. Malone and M. L. Cohen, J. Phys.: Cond. Matter **25**, 105503 (2013).